Optica Applicata, Vol. LIII, No. 3, 2023
DOI: 10.37190/oa230312

Common path optical coherence tomography with electronic feedback for improved sensitivity

KHALID ALSNAIE

Electrical Engineering Department, Faculty of Engineering,
Imam Mohammad Ibn Saud Islamic University, Riyadh, KSA

Optical coherence tomography (OCT) imaging has become a useful tool in medical diagnosis over the past 25 years, because of its ability to visualize intracellular structures at high resolution. The main objective of this work is to add electronic feedback to the optical coherence tomography setup to increase its sensitivity. Noise added to the measured interferogram obscures some details of examined tissue layered structure. Adjusting signal power level in such a way to improve signal-to-noise ratio can help to enhance image quality. Electronic feedback is added to enhance system sensitivity. A logarithmic amplifier is included in the OCT setup to automatically adapt signal level. Moreover, the resolution of the optical spectrum analyzer is controlled according to the farthest layer detected in the A-scan. These techniques are tested showing an improvement in obtained image of a human nail.

Keywords: optical coherence tomography, frequency domain OCT, medical imaging, partially coherent interferometers, B-scan.

1. Introduction

Optical coherence tomography (OCT) is a noninvasive imaging technique which generates *in vivo* cross-sectional images of tissues with high resolution. First reported in the 1990s, OCT has been one of the most successful technologies adopted and applied in various investigational and clinical fields. Due to a physical limitation arising from the need to a moving mirror in the early setup, the scanning speed was limited to 400 axial scans (A-scans)/s. OCT uses low coherence interferometry to obtain A-scan intensity profiles, and the process requires light to be split and sent to both a reference arm with a mirror and to the sample. Interference between reflected beams from a reference arm and the tissue occurs if the path length to the reference mirror and tissue match to within the coherence length of the light source. This interference pattern in wavelength domain is called an interferogram. Intensity information, in the form of a reflectivity profile in depth of the examined tissue, can be extracted from the interferogram. Changing the location of the reference mirror allows backscattered tissue intensity levels to be detected from different depths in the tissue sample. This approach is referred to as time-domain (TD)-OCT because time-encoded signals are obtained directly. Several improvements in OCT hardware have been introduced since

the first commercial TD-OCT system became available. Better axial resolution [1,2] and increased scanning speed [2-4] are the two main advancements that have recently become incorporated into commercial systems. The implementation of broadband light sources into OCT systems [1] improved the axial resolution from ~10 μm to as high as 2 μm in tissue [3] Acquisition speed has improved considerably by detecting backscattering signals in the frequency domain [2-4], which means backscattered depth information at a given location can be collected without the movement of a reference mirror. The first *in vivo* tomograms of human retina are obtained by Fourier domain optical coherence tomography in 2002 [2]. Frequency information is acquired with a broad-bandwidth light source, charge-coupled device (CCD) camera, and a spectrometer [2,3] or by sweeping a narrow-bandwidth source through a broad range of frequencies with a photodetector [4]. The approach that incorporates a broadband light source is often referred to as frequency-domain (FD)-OCT, whereas the latter is termed swept-source (SS)-OCT [5,6]. In both approaches, intensity profiles (A-scans) are obtained using a Fourier transform of the detected frequencies, and this facilitates rapid A-scan collection. In addition to improved scanning speed, FD-OCT also offers the advantage of higher detection sensitivity, that is, it exhibits higher signal-to-noise, given a perfect reflector [3-4].

One of the drawbacks of FD-OCT is autocorrelation noise arising due to the interference among signals reflected from different tissue layers. Imaginary layers in the produced image are the result of this autocorrelation noise that obscures some of the image details [7]. The differential Fourier domain method dFD-OCT employs the fact that terms carrying direct information on the location of reflecting layers depend on the reference mirror position while the remaining parasitic terms do not. In order to completely remove the parasitic terms, it is sufficient to measure one additional spectrum with a phase shift π introduced into the reference arm. After subtraction of these two spectra, one yields terms associated exclusively with the object structure [2]. The Fourier transform of the measured interferogram produces two mirror reversed images and hence halves the imaging range. In a way to solve this problem [8] proposed shifting the reference arm to obtain a second interferogram for the same A-scan. With the help of these two interferogram recordings, the imaging range is doubled.

Noise accumulated on the measured interferogram degrades image quality since noise transforms from the wavelength-domain to the depth-domain. System sensitivity of detecting tissue layers depends strongly on level of signal-to-noise ratio. The sensitivity is defined as the reciprocal of the smallest sample reflectivity for which the S/N ratio equals to one [9].

SS-OCT and FD-OCT have equivalent expressions for system signal-to-noise ratio which result in a typical sensitivity advantage of 20–30 dB over TD-OCT. The sensitivity of FD-OCT and SS-OCT is independent of source bandwidth and scan depth while that of TD-OCT depends. The result of analyzing and simulating with a numerical model, the OCT signal-to-noise ratio in the frequency-domain (shot noise limited) shows that actual systems have 6.7 dB higher values of signal-to-noise ratio [10]. In case of FD-OCT, the total reference power needed to achieve shot noise-limited de-

tection simultaneously on all photodetectors of the optical spectrum analyzer is more than that needed for SS-OCT and TD-OCT by a factor of M where M is the number of photodetectors [4]. Signal-to-noise ratio S/N of the acquired signal is related to the system dynamic range DR. The dynamic range of OCT system is related to the maximum signal-to-noise ratio S/N_{max} by $DR = 10\log(S/N_{max})$ [2]. Signal-to-noise ratio for a system dominated by shot noise is

$$\mathrm{SNR}_{\mathrm{shot}} = \frac{I_{\mathrm{ph}}^2}{\sigma_{\mathrm{shot}}^2} = \frac{(RP_{\mathrm{ph}})^2}{2q(RP_{\mathrm{ph}})B} = \frac{RP_{\mathrm{ph}}}{2qB} \tag{1}$$

where I_{ph} is the current produced by the photodetection process, σ_{shot}^2 is the shot noise power, P_{ph} is the optical power, R is the detector responsivity, B is the system bandwidth, and q is the electron charge. It is apparent that signal-to-noise ratio is proportional to the optical power. Hence in a system dominated by shot noise, increasing optical power enhances signal-to-noise ratio.

In this study, electronic feedback is employed to increase system sensitivity by two ways. The first approach is to add a logarithmic amplifier to control the output power level from the super-luminescent light emitting diode according to the level of the reflected signal of the tissue layers. The second is to adapt the resolution of the optical spectrum analyzer based on detecting the farthest layer of the A-scan of the tissue sample.

This work is organized as follows. 1) Test the proposed electronic feedback on a sample composed of three glass microscope slides stacked together with a small air gap between each glass slide and its adjacent one and compare with the obtained image without employing feedback. 2) Compare the image obtained with and without feedback by examining a human nail.

2. Proposed OCT system

Figure 1 shows the basic block diagram of a common path FD-OCT system where a super-luminescent light emitting diode with a broad spectral width output is split using a 50:50 optical fiber coupler. The reflected signal of the fiber probe tip (reference signal) along with reflected signals of tissue layers, comprising the interferogram, are

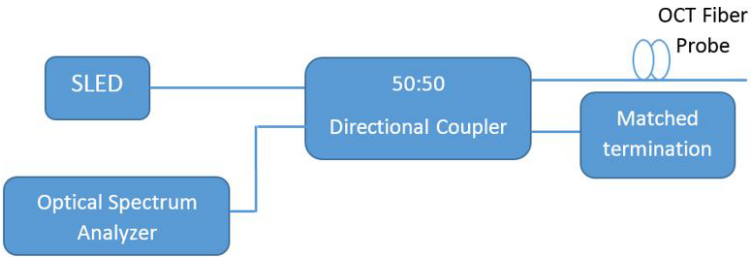

Fig. 1. Common path OCT basic block diagram.

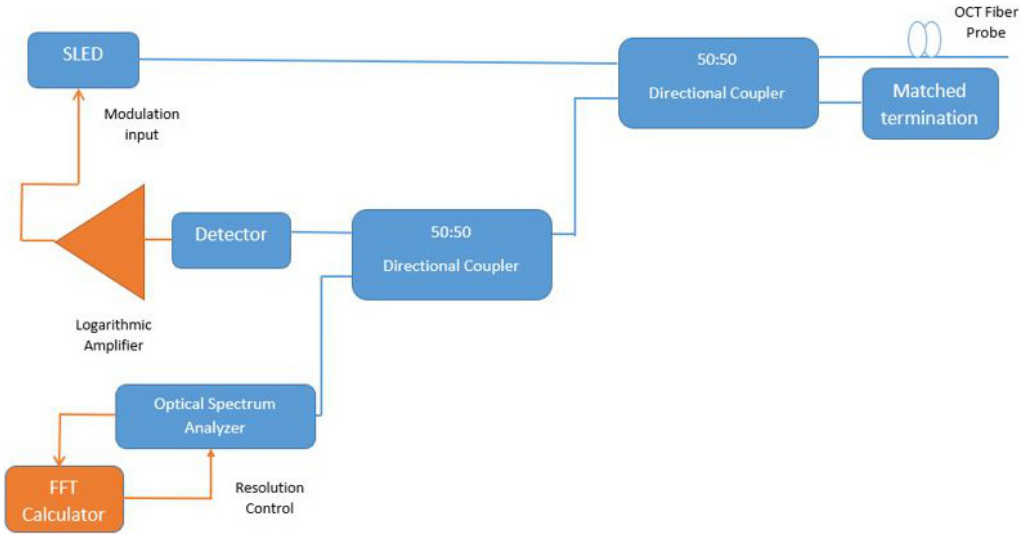

Fig. 2. Proposed OCT block diagram with electronic feedback.

coupled back to the optical spectrum analyzer OSA. Processing the interferogram signal gives the structure of the examined tissue.

Figure 2 shows the proposed setup with the addition of an electronic feedback which is a detector with a transimpedance amplifier followed by a logarithmic amplifier and an inverting amplifier.

An op-amp based logarithmic amplifier produces a voltage at the output, which is proportional to the logarithm of the voltage that is applied to the inverting terminal of the op-amp. The circuit diagram of a logarithmic amplifier followed by an inverting amplifier is shown in Fig. 3.

The overall output of the two cascaded amplifiers is given as

$$V_0 = \frac{R_2}{R_1} V_T \log_e\left(\frac{V_{in}}{I_S R}\right) \tag{2}$$

Note that, in the above equation the parameters V_T and I_S are constants where V_T is the temperature equivalent voltage, which is equal to 26 mV at room temperatur and

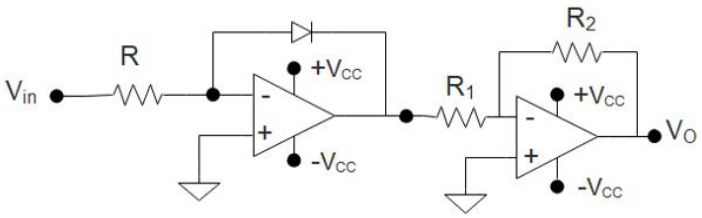

Fig. 3. The circuit diagram of the logarithmic amplifier followed by an inverting amplifier.

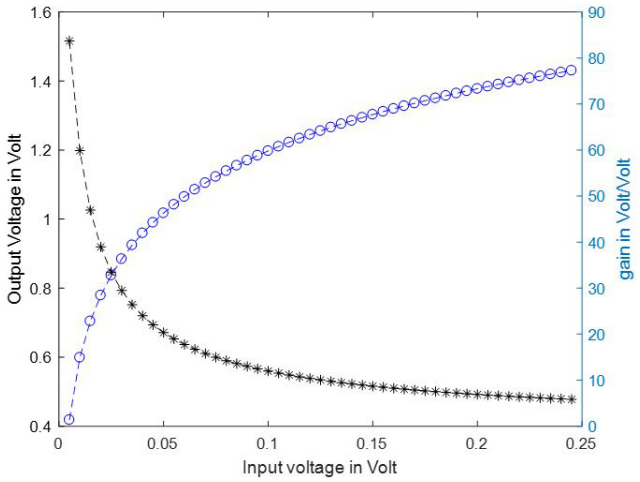

Fig. 4. The output voltage of the cascaded amplifiers of Fig. 3 *vs*. input voltage (marked by asterisk), and its gain *vs*. input voltage (marked by circles).

I_S is the diode reverse saturation current which is in the order of nanoamperes. So, the output voltage V_0 will be proportional to the natural logarithm of the input voltage V_{in}.

Figure 4 shows the voltage output of these cascaded amplifiers against its input voltage for the following parameters: $R = 100\ \text{k}\Omega$, $R_1 = 1\ \text{k}\Omega$, $R_2 = 10\ \text{k}\Omega$, and $I_S = 10\ \text{nA}$.

3. Tradeoff between optical resolution of optical spectrum analyzer and system sensitivity

In a second stage, as Fig. 2 shows, the resolution of the optical spectrum analyzer (OSA) is controlled according to the farthest layer detected of the A-scan of the sample. A threshold determines whether a layer is detected according to its level with respect to the noise floor. Upon determining the layer that is at a maximum depth away from the surface of the sample, the feedback controls the resolution of the acquired signal from the OSA. Reducing the OSA resolution when it is not necessary to keep it at its maximum value reduces the amount of collected noise and hence increases system sensitivity.

4. Mathematical modeling of OCT system

FD-OCT acquires the spectral interferogram $I(\lambda)$ spectrally resolved which is given by

$$I(\lambda) = \sum_{i=1}^{m} R_i + 2\sqrt{R_0 R_i}\cos(2kd_i) + 2\sqrt{R_i R_{i+1}}\cos\left[2k(d_{i+1} - d_i)\right] \tag{3}$$

where $I(\lambda)$ is the interferogram in λ domain, m is the number of layers, R_i is the reflection coefficient of layer i, R_0 is the reflection coefficient of the reference signal arising

from the fiber probe tip in common path OCT configuration, k is the wave number given as $k = 2\pi/\lambda$. First term of equation contributes to DC component, the second term represents actual layers existing at distances d_i from the fiber probe tip. The third term contributes to autocorrelation noise.

One of important parameter of OCT systems is axial resolution which is determined by the linewidth of the used light source and is given by:

$$\Delta L = \frac{2\ln(2)}{\pi} \frac{\lambda_o^2}{\Delta\lambda} \tag{4}$$

where λ_o is the central wavelength of the light source and $\Delta\lambda$ is its spectral full-width at half-maximum (FWHM). Increasing light source linewidth improves axial resolution [1,2]. Axial resolution of 2.5 μm and 10000 A-scans/sec using femtosecond pulsed titanium:sapphire laser at 800 nm equipped with a 100 m dispersive fiber resulting in a 120 nm (FWHM) linewidth is achieved [11]. Subcellular imaging with longitudinal resolution of approx. 1 μm in tissue is achieved [1]. Axial resolution of OCT systems is deteriorated due to dispersion of examined tissues [10].

To show clearly the layers of the sample, we follow the following steps.

1) The interferogram captured from the OSA in wavelength domain is first converted to frequency domain. This step renders the interferogram frequency axis spacing to be nonlinear.

2) The new interferogram is then treated by interpolation to adjust the spacing between sampling points (constant spacing in frequency axis). Steps 1 and 2 can be avoided if an interferogram is captured with a linear-in-wave-number spectrometer, which has an impact on accelerating display rates of OCT images [12].

3) Finally by using FFT transform, the layers structure of the studied sample is obtained. The depth axis is multiplied by $\frac{1000}{\Delta f}\frac{c}{2}$ to show the location of these layers in millimeters.

5. Results and discussions

The idea of feedback control of the output power level from the SLD is interesting for human safety aspects, and to avoid detector saturation. The new system is first tested using a sample composed of three glass microscope slides stacked together and separated by a small air gap. To quantify the dependence of the measured signal-to-noise ratio on the output level of the super-luminescent SLED source, the bias current of the SLED is changed manually. The level of the signal-to-noise ratio at each value of the SLED bias current are measured. For this sample, the ratio between the measured signal level reflected of the first sample surface to the highest noise level is calculated while varying SLED bias current. Figure 5 shows that the signal-to-noise ratio increases as the bias current and hence the incident optical power increase.

Figure 6 shows the A-scan obtained for the layers of this sample without applying the feedback whereas Fig. 7 shows the same sample when feedback is operating. It is

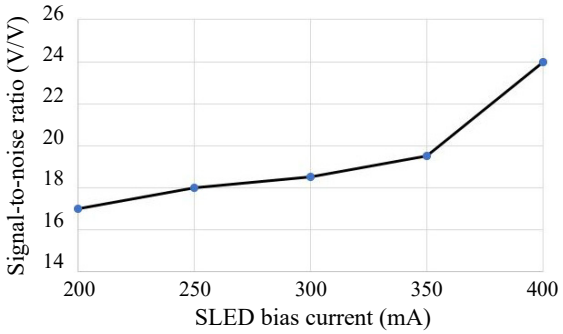

Fig. 5. The detected signal-to-noise ratio for different values of SLED bias current.

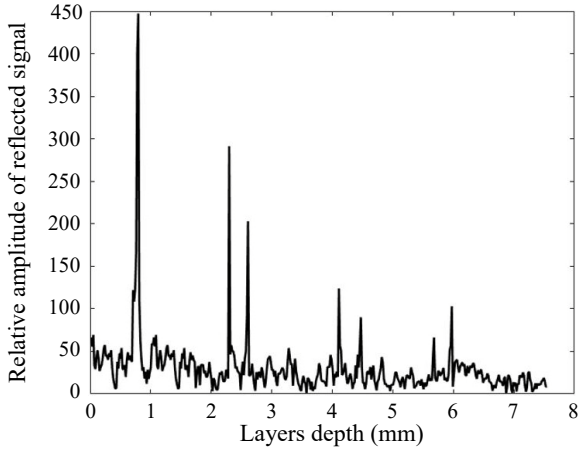

Fig. 6. The A-scan showing the structure of the sample composed of three glass microscope slides separated by small air gap measured with the OCT system without feedback.

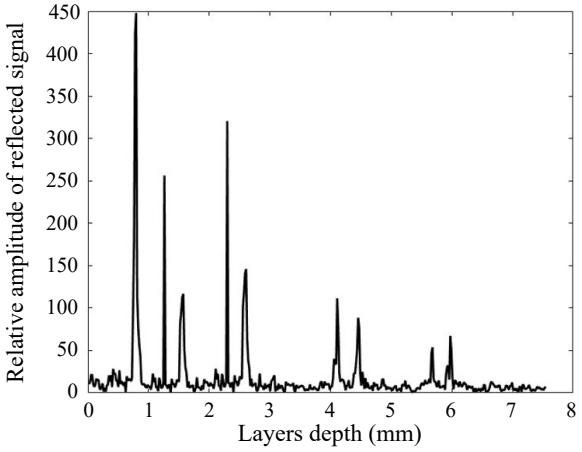

Fig. 7. The same as in Fig. 4 when applying electronic feedback.

clear that electronic feedback increased to a great extent the signal-to-noise ratio. In Figs. 6 and 7, the DC component produced by the FFT algorithm is removed to clearly show the reflected signals from sample layers. The level of the reflected signal of the first surface of the sample in Figs. 6 and 7 is then made equal for comparing the noise level with and without the application of feedback. The used optical spectrum analyzer from Yokogawa has a sweeping speed of 0.2 sec/100 nm.

Figures 8 and 9 show the B-scan of the same sample without and with feedback, respectively. It is evident that without applying feedback some details of the image

Fig. 8. The B-scan showing the structure of the sample composed of three glass microscope slides separated by small air gap measured with the OCT system without feedback.

Fig. 9. The same as in Fig. 7 when applying electronic feedback.

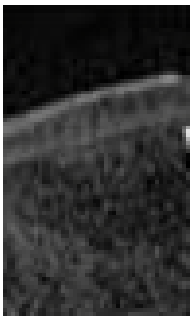

(a)

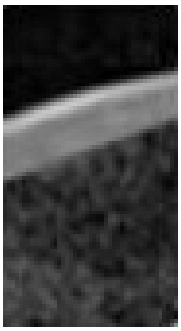

(b)

Fig. 10. Part of a human nail showing the dorsal and the intermediate layers and the dermis (a) without resolution control, and (b) with resolution control.

are obscured by the high level of noise. Lateral scanning is accomplished by mounting the OCT probe on a stage driven by a stepper motor.

In the second test we examined a human nail. The B-scan of this nail is shown in Fig. 10(a) without feedback, and the same is shown in Fig. 10(b) when applying feedback. Again it is obvious that applying feedback enhanced image quality.

6. Conclusions

In this work a method to enhance image clarity using electronic feedback by increasing signal-to-noise ratio is implemented. The impact of additive noise is to obscure some of the details of the sample under test in OCT setup. The proposed technique is to add electronic feedback to increase SLED signal level when reflected signal of tissue layers is small in an adaptive manner and also to control the resolution of the optical spectrum analyzer. A group of readings was taken from the first sample and the result of the A-scan and the B-scan showed a better image clarity. In a second stage, the setup with and without feedback was tested on a human nail showing its layers. Electronic feedback impact on image was evident where SNR amelioration was emphasized.

Acknowledgment
The authors would like to thank the Deanship of Scientific Research at Imam Mohammad Ibn Saud Islamic University for the continuous help during this work by providing the space and equipment required to carry out the experimental measurements.

References

[1] Drexler W., Morgner U., Kartner F.X., Pitris C., Boppart S.A., Li X.D., Ippen E.P., Fujimoto J.G., *In vivo ultrahigh-resolution optical coherence tomography*, Optics Letters **24**(17), 1999: 1221-1223. https://doi.org/10.1364/OL.24.001221

[2] Wojtkowski M., Leitgeb R., Kowalczyk A., Bajraszewski T., Fercher A., *In vivo human retinal imaging by Fourier domain optical coherence tomography*, Journal of Biomedical Optics **7**(3), 2002: 457-463. https://doi.org/10.1117/1.1482379

[3] Wojtkowski M., Srinivasan V., Fujimoto J.G., Ko T., Schuman J.S., Kowalczyk A., Duker J.S., *Three-dimensional retinal imaging with high-speed ultrahigh resolution optical coherence tomography*, Ophthalmology **112**(10), 2005: 1734-1746. https://doi.org/10.1016/j.ophtha.2005.05.023

[4] Choma M.A., Sarunic M.V., Yang C., Izatt J.A., *Sensitivity advantage of swept source and Fourier domain optical coherence tomography*, Optics Express **11**(18), 2003: 2183-2189. https://doi.org/10.1364/OE.11.002183

[5] Targowski P., Bajraszewski T., Gorczyńska I., Góra M., Szkulmowska A., Szkulmowski M., Wojtkowski M., Kaluzny J.J., Kaluzny B.J., Kowalczyk A., *Spectral optical coherence tomography for nondestructive examinations*, Optica Applicata **36**(4), 2006: 609-619.

[6] Heindl L.M., Siebelmann S., [Eds.], *Optical Coherence Tomography of the Anterior Segment*, Springer, 2022.

[7] De Boer J.F., *Spectral/Fourier domain optical coherence tomography*, [In] *Optical Coherence Tomography. Biological and Medical Physics, Biomedical Engineering*, [Eds.] Drexler W., Fujimoto J.G., Springer, Berlin, Heidelberg, 2008.

[8] Szkulmowski M., Bajraszewski T., Szkulmowska A., Targowski P., Kowalczyk A., *Efficient residual error reduction in complex spectral optical coherence tomography with arbitrary or unknown phase*, Optica Applicata **36**(1), 2006: 147-155.

[9] DE BOER J.F., LEITGEB R., WOJTKOWSKI M., *Twenty-five years of optical coherence tomography: The paradigm shift in sensitivity and speed provided by Fourier domain OCT*, Biomedical Optics Express **8**(7), 2017: 3248-3280. https://doi.org/10.1364/BOE.8.003248

[10] KALKMAN J., *Fourier-domain optical coherence tomography signal analysis and numerical modeling*, International Journal of Optics, Vol. 2017, March 2017: 9586067. https://doi.org/10.1155/2017/9586067

[11] LEITGEB R.A., DREXLER W., UNTERHUBER A., HERMANN B., BAJRASZEWSKI T., LE T., STINGL A., FERCHER A.F., *Ultrahigh resolution Fourier domain optical coherence tomography*, Optics Express **12**(10), 2004: 2156-2165. https://doi.org/10.1364/OPEX.12.002156

[12] WATANABE Y., ITAGAKI T., *Real-time display on Fourier domain optical coherence tomography system using a graphics processing unit*, Journal of Biomedical Optics **14**(6), 2009: 060506. https://doi.org/10.1117/1.3275463

Received February 11, 2023
in revised form March 3, 2023